JOC Featured Article

pubs.acs.org/joc

Tandem [8 + 2] Cycloaddition−[2 + 6 + 2] Dehydrogenation Reactions Involving Imidazo[1,2-*a*]pyridines and Imidazo[1,2-*a*]pyrimidines

Maialen Aginagalde,[†] Yosu Vara,[‡] Ana Arrieta,[†] Ronen Zangi,[†,§] Vicente L. Cebolla,[⊥] Arantzazu Delgado-Camón,[⊥] and Fernando P. Cossío*,[†]

[†]*Kimika Organikoa I Saila, Universidad del País Vasco-Euskal Herriko Unibertsitatea (UPV-EHU), P. K. 1072, 20018 San Sebastián-Donostia, Spain,* [‡]*Ikerchem Ltd., Tolosa Etorbidea 72, 20018 San Sebastián-Donostia, Spain,* [§]*Ikerbasque, Basque Foundation for Science 48011 Bilbao, Spain, and* [⊥]*Instituto de Carboquímica, Consejo Superior de Investigaciones Científicas (CSIC), Miguel Luesma Castán 4, 50018 Zaragoza, Spain*

fp.cossio@ehu.es

Received November 4, 2009

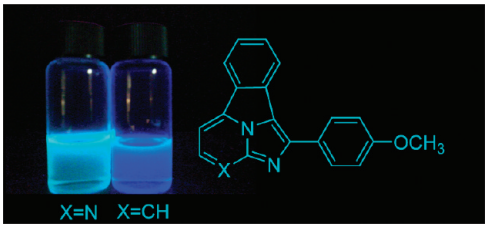

The reaction between benzynes and imidazo[1,2-*a*]pyridines (pyrimidines) to form benzo[*a*]imidazo-[5,1,2-*cd*]indolizines and 2,3,9c-triazocyclopenta[*j*,*k*]fluorenes has been studied computationally and experimentally. It is found that these reactions take place via tandem [$_{\pi}8_{s} + {}_{\pi}2_{s}$] and [$_{\sigma}2_{s} + {}_{\pi}6_{s} + {}_{\sigma}2_{s}$] processes. The [8 + 2] cycloaddition steps are essentially barrierless, and the aromatization steps occur via highly synchronous aromatic transition structures. From an experimental standpoint, the reaction is feasible under microwave irradiation and using 2-(trimethylsilyl)phenyl triflates as benzyne precursors. Depending on the substitution pattern in the starting triflate a complete regiocontrol of the reaction can be achieved. The tetracyclic compounds thus prepared emitted blue light when excited at 365 nm and exhibited interesting photophysical properties.

Introduction

The Woodward−Hoffmann rules for thermal cycloadditions predict that allowed supra−supra reactions require 4n + 2π-electrons in the reacting system.[1] Whereas thermal cycloadditions with $n = 1$ have been extensively studied, the extension to $n = 2$ has been explored into a much lesser extent.[2] Several [$_{\pi}8_{s} + {}_{\pi}2_{s}$] thermal cycloadditions have been studied, most of them involving 7-methylenecyclohepta-1,3,5-triene[3] and heteroanalogous 5,7-dimethylenecyclohepta-1,3-diene[4] and indolizines.[5,6] In many cases, aromatized products are obtained.[5,6] This aromatization step is related to thermally allowed cycloadditions involving hydrogen and aromatic hydrocarbons and heterocycles, a process that has attracted the interest of different research groups.[7]

Recently, our group has published[8] the preparation of 1*H*-indoles, imidazo[1,2-*a*]pyridines, and imidazo[1,2*a*]pyrimidines.

(1) Woodward, R. B.; Hoffmann, R. *Angew. Chem., Int. Ed. Engl.* **1969**, *8*, 781–853.

(2) (a) Nair, V.; Abhilash, K. G. *Synlett* **2008**, 301–312. (b) Sankararaman, S. *Pericyclic Reactions −A Textbook*; Wiley-VCH: Weinheim, 2005; pp 193−196.

(3) (a) Doering, W. v. E.; Wiley, D. W. *Tetrahedron* **1960**, *11*, 183–198. (b) Rigby, J. H.; Ahmed, G.; Ferguson, M. D. *Tetrahedron Lett.* **1993**, *34*, 5397–5400. (c) Rigby, J. H.; Pigge, F.-C.; Ferguson, M. D. *Tetrahedron Lett.* **1994**, *35*, 8131–8132. (d) Machiguchi, T.; Yamabe, S. *Tetrahedron Lett.* **1990**, *31*, 4169–4172. (e) Ito, K.; Saito, K.; Takahashi, K. *Bull. Chem. Soc. Jpn.* **1992**, *65*, 812–816. (f) Nair, V.; Abhilash, K. G. *Tetrahedron Lett.* **2006**, *47*, 8707–8709.

(4) Farrant, G. C.; Feldman, R. *Tetrahedron Lett.* **1970**, *11*, 4979–4982.

(5) See, for example: (a) Galbraith, A.; Small, T.; Barnes, R. A.; Bockelheide, V. *J. Am. Chem. Soc.* **1961**, *83*, 453–456. (b) Kuznetsov, A. G.; Bush, A. K.; Babaev, E. V. *Tetrahedron* **2008**, *64*, 749–756.

(6) (a) Mitsumori, T.; Benoikov, M.; Dautel, O.; Wudl, F.; Shioya, T.; Sato, H.; Sato, Y. *J. Am. Chem. Soc.* **2004**, *126*, 16793–16803. (b) Shen, Y.-M.; Grampp, G.; Leesakul, N. L.; Hu, H.-W.; Xu, J.-H. *Eur. J. Org. Chem.* **2007**, 3718–3726.

(7) (a) Hayden, A. E.; Houk, K. N. *J. Am. Chem. Soc.* **2009**, *131*, 4084–4089. (b) Zhong, G.; Chan, B.; Radom, L. *J. Am. Chem. Soc.* **2007**, *129*, 924–933.

(8) Vara, Y.; Aldaba, E.; Arrieta, A.; Pizarro, J. L.; Arriortua, M. I.; Cossio, F. P. *Org. Biomol. Chem.* **2008**, *6*, 1763–1772.

Published on Web 11/18/2009 DOI: 10.1021/jo9022815

SCHEME 1. Reaction between Imidazo[1,2-*a*]pyridine 1a or Imidazo[1.2-*a*]pyrimidine 1b and Benzine 2 to Yield [8 + 2] Cycloadducts 3a,b and Dehydrogenated Products 4a,b

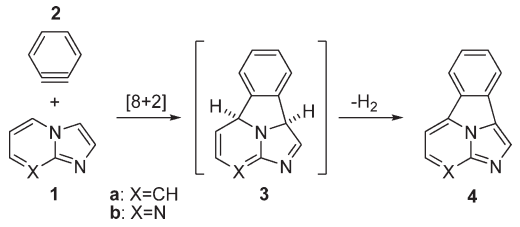

Given the generality of these reactions, we reasoned that the two last families of bicyclic heterocycles **1** could be suitable substrates for [8 + 2] cycloadditions (Scheme 1). Since the starting molecules **1** must lose aromaticity to yield [8 + 2] cycloadducts **3**, we decided to use benzynes as tetraenophiles since these highly reactive compounds should provide tetracyclic compounds **3a**,**b** efficiently. We expected that these intermediates should aromatize to yield benzo[*a*]imidazo[5,1,2-*cd*]indolizines **4a** and 2,3,9c-triazocyclopenta[*j*,*k*]fluorenes **4b**. In addition, the interesting photophysical properties reported for indolizino-[3,4,5-*ab*]isoindoles[6] constitute a stimulus to prepare compounds **4a**,**b** and to investigate the nature of the [$_{\pi}8_s$ + $_{\pi}2_s$] and [$_{\sigma}2_s$ + $_{\pi}6_s$ + $_{\sigma}2_s$] thermal processes required for their formation.

Within this context, in this paper we describe the mechanism of the [$_{\pi}8_s$ + $_{\pi}2_s$] reaction between compounds **1** and benzynes as well as the conversion of intermediates **3** in compounds **4**. Next, we describe the preparation of 1-substituted derivatives of **4a**,**b** via microwave-assisted reaction between benzyne precursors and imidazo[1,2-*a*]pyridines and imidazo[1,2-*a*]pyrimidines. Finally, the photophysics of the final compounds thus prepared will be discussed.

Computational Methods

All the time-independent computational studies reported in this work were performed using the Gaussian 03[9] and Jaguar[10] programs, within the density functional theory (DFT) framework.[11] Both B3LYP[12] and M06-2X[13] hybrid functionals were used along with the 6-31G* split-valence basis set.[14] The accuracy of both methods has been extensively tested[15,16] for stable molecules and pericyclic reactions. Wiberg bond indices[17] were computed using the NBO method.[18] Nucleus-independent chemical shifts (NICS)[19] were computed on B3LYP/6-31G* geometries using the GIAO method.[20]

The synchronicities[21] of several reactions were quantified according to eq 1,[22]

$$\mathrm{Sy} = 1 - \frac{1}{2n-2}\sum_{i=1}^{n}\frac{|\delta B_i - \delta B_{av}|}{\delta B_{av}} \quad (1)$$

where n is the number of bonds being modified along the reaction coordinate and δB_i is the variation of the bond index of a given atom pair i on going from the reactants (R) to the products (P) via the corresponding transition structure (eq 2):

$$\delta B_i = \frac{B_i^{TS} - B_i^{R}}{B_i^{P} - B_i^{R}} \quad (2)$$

The average value δB_{av} is given by eq 3:

$$\delta B_{av} = n^{-1}\sum_{i=1}^{n}\delta B_i \quad (3)$$

According to these definitions, for a perfectly synchronous reaction a value of Sy = 1 is achieved.

All the stationary points were characterized by harmonic analysis.[23] Activation energies (ΔE_a) and reaction energies (ΔE_{rxn}) were computed including zero-point vibrational energy (ZPVE) corrections.

Car−Parrinello simulations[24] of the intermediate structure **3a** were performed using the Quantum Espresso package.[25] The norm-conserving pseudopotentials C.BLYP-mt.UPF, N. BLYP-mt.UPF, and H.BLYP-vbc.UPF, obtained from the Quantum Espresso distribution, were used to describe the interaction between the core and valence electrons in carbon, nitrogen, and hydrogen atoms, respectively. The valence wave functions were expanded in a plane wave basis set with an energy cut off in the range 40−100 Ry. The exchange-correlation functional was approximated by the BLYP method.[26] The electrons were assigned a fictitious mass of 400 au. The simulations were performed in the NVT ensemble, where the temperature was controlled by the Nosé−Hoover chain thermostat,[27] and $V = 11.642^3$ Å^3 = 1577.87 Å^3. After reaching the electronic ground state, the "ionic" positions were energy minimized using the steepest descent algorithm. Then the "ionic" and electronic degrees of freedom were propagated using the velocity−Verlet algorithm[28] and the former gradually (using simulations at T = 50, 100, 200, and 300 K) heated to T = 400 K.

Results and Discussion

First, we analyzed the possible reactions paths leading to [8 + 2] cycloadducts **3a**,**b** starting from compounds **1a**,**b** and

(9) *Gaussian 03, Rev E.01*; Frisch, M. J., Ed.; et al. Gaussian, Inc.: Wallingford, CT, 2004.
(10) *Jaguar, version 7.5*; Schrödinger, LLC: New York, 2008.
(11) (a) Parr, R. G.; Yang, W. *Density-Functional Theory of Atoms and Molecules*; Oxford University Press: Oxford, 1989. (b) Ziegler, T. *Chem. Rev.* **1991**, *91*, 651–667.
(12) (a) Kohn, W.; Becke, A. D.; Parr, R. G. *J. Phys. Chem.* **1996**, *100*, 12974–12980. (b) Becke, A. D. *J. Chem. Phys.* **1993**, *98*, 5648–5652. (c) Becke, A. D. *Phys. Rev. A* **1988**, *38*, 3098–3100.
(13) Zhao, Y.; Truhlar, D. G. *Theor. Chem. Acc.* **2008**, *120*, 215–241.
(14) Hehre, W. J.; Radom, L.; Schleyer, P. v. R.; Pople, J. A. *Ab Initio Molecular Orbital Theory*; Wiley: New York, 1986; pp 76−87 and references cited therein.
(15) Guner, V.; Khuong, K. S.; Leach, A. G.; Lee, P. S.; Bartberger, M. D.; Houk, K. N. *J. Phys. Chem. A* **2003**, *107*, 11445–11459.
(16) (a) Zhao, Y.; Truhlar, D. G. *Acc. Chem. Res.* **2008**, *41*, 157–167. (b) Chen, J.-L.; Hong, J.-T.; Wu, K.-J.; Hu, W.-P. *Chem. Phys. Lett.* **2009**, *468*, 307–312.
(17) Wiberg, K. B. *Tetrahedron* **1968**, *24*, 1083–1096.
(18) (a) *NBO 5.0*: Glendening, E. D.; Badenhoop, J. K.; Reed, A. E.; Carpenter, J. E.; Bohmann, J. A.; Morales, C. M.; Weinhold, F., Theoretical Chemistry Institute, University of Wisconsin: Madison, **2001**. (b) Reed, A. E.; Curtiss, L. A.; Weinhold, F. *Chem. Rev.* **1988**, *88*, 899–926. (c) Reed, A. E.; Weinstock, R. B.; Weinhold, F. *J. Chem. Phys.* **1985**, *83*, 735–746.
(19) Schleyer, P. v. R.; Maerker, C.; Dransfeld, A.; Jiao, H.; Hommes, N. S. R. v. E. *J. Am. Chem. Soc.* **1996**, *118*, 6317–6318.
(20) Wolinski, K.; Hilton, J. F.; Pulay, P. *J. Am. Chem. Soc.* **1990**, *112*, 8251–8260.
(21) Borden, W. T.; Loncharich, R. J.; Houk, K. N. *Annu. Rev. Phys. Chem.* **1988**, *39*, 213–236.
(22) (a) Moyano, A.; Pericàs, M. A.; Valentí, E. *J. Org. Chem.* **1989**, *54*, 573–582. (b) Lecea, B.; Arrieta, A.; Lopez, X.; Ugalde, J. M.; Cossío, F. P. *J. Am. Chem. Soc.* **1995**, *117*, 12321–12314.
(23) McIver, J. W. Jr.; Komornicki, A. J. *J. Am. Chem. Soc.* **1972**, *94*, 2625–2633.
(24) Car, R.; Parrinello, M. *Phys. Rev. Lett.* **1985**, *55*, 2471–2474.
(25) Baroni, S.; Dal Corso, A.; De Gironcoli, S.; Giannozzi, P.; Cavazzoni, C.; Ballabio, G.; Scandolo, S.; Chiarottí, G.; Focher, P.; Pasquarello, A.; Lasonen, K.; Trave, A.; Car, R.; Marzari, N.; Kokalj, A. *Quantum Espresso Package 2005*, http://www.quantum-espresso.org, accessed March 26, 2009.
(26) (a) Becke, A. D. *J. Chem. Phys.* **1992**, *96*, 2155–2160. (b) Lee, C.; Yang, W.; Parr, R. G. *Phys. Rev. B* **1988**, *37*, 785–789.
(27) (a) Nosé, S. *Mol. Phys.* **1984**, *52*, 255–268. (b) Hoover, W. G. *Phys. Rev. A* **1985**, *31*, 1695–1697.
(28) Verlet, L. *Phys. Rev.* **1967**, *159*, 98–103.

SCHEME 2. Possible Pericyclic Reaction Paths in the Thermal Reaction between 1a,b and 2 To Form Tetracyclic Compounds 4a,b

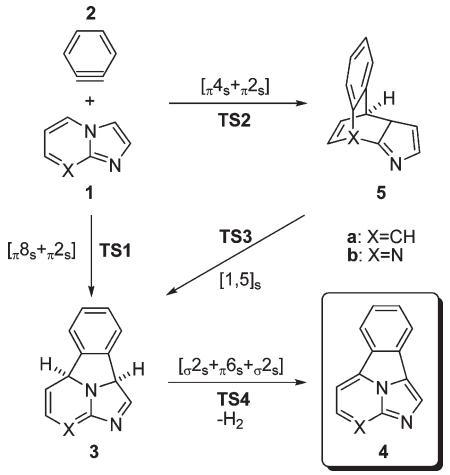

benzyne **2** (Scheme 1). In principle, tetracyclic compounds **3a**,**b** can be formed via thermally allowed [$_{\pi}8_s$ + $_{\pi}2_s$] concerted cycloadditions (Scheme 2). Alternatively a [$_{\pi}4_s$ + $_{\pi}2_s$] cycloaddition can be envisaged. The intermediate [4 + 2] cycloadducts **5a**,**b** thus formed can be transformed into products **3a**,**b** via thermal [1,5]$_s$ sigmatropic shifts. Finally, the [$_{\sigma}2_s$ + $_{\pi}6_s$ + $_{\sigma}2_s$] reactions of **3a**,**b** yield the dehydrogenated products **4a**,**b**.

Inspection of the relevant orbitals[29] of **1a** and **2** (Figure 1) shows that the main contact between both reactants involves a two-electron interaction between the HOMO of **1a** and the b_2-symmetric LUMO of **2**. It is noteworthy that both the [8 + 2] and the [4 + 2] interaction modes are topologically allowed since both the Ca−C5/Cb−C3, and Ca−C5/Cb−C8 HOMO−LUMO combinations are in-phase (Figure 1). However, the HOMO expansion coefficient of C8 is lower than that of C3. The other two-electron interaction is less favorable and involves the LUMO of **1a** and the a_1-symmetric HOMO-1 of **2**. In this case, the energy gap between both MOs is larger than in the former interaction. In addition, there is no noticeable coefficient for C3 in the LUMO, whereas the expansion coefficient of C5 is high and allows an in-phase interaction with the HOMO-1 of **2**. This two-electron interaction should result in a relatively asynchronous mechanism for the [8 + 2] cycloaddition.

Both [8 + 2] and [4 + 2] transition structures **TS1a** and **TS2a** were located and characterized at the B3LYP/6-31G* level. The chief geometric features of these saddle points are gathered in Figure 2. As predicted, **TS1a** is found to be quite asynchronous, the Cb−C3 bond distance being significantly shorter than that corresponding to Ca−C5.The computed synchronicity for the **1a** + **2** → **3a** transformation via **TS1a** is Sy = 0.67, which corresponds to a very asynchronous process. It was found that the [8 + 2] reaction between **1a** and **2** is essentially barrierless in terms of total energy using both B3LYP and M06-2X hybrid functionals, the activation free energy being larger. In order to estimate the possible

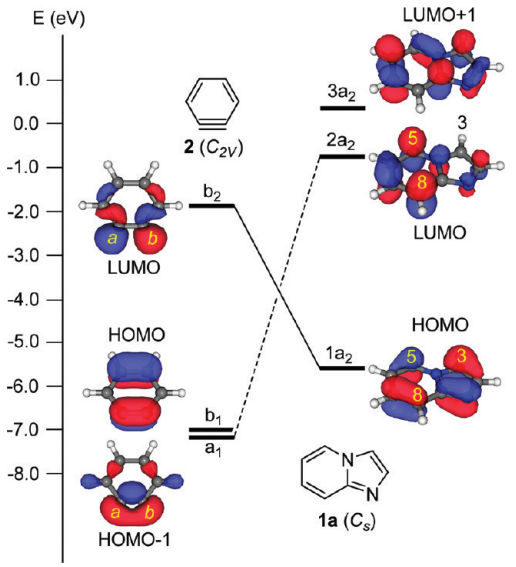

FIGURE 1. Kohn−Sham molecular orbitals of **1a** and **2**, calculated at the B3LYP/6-31G* level.

biradical character of **TS1a**, we performed a CASSCF(4,4)/6-31G* calculation at the B3LYP/6-31G* geometry. The occupancies of the natural orbitals of the active space were calculated to be 1.939, 1.825, 0.175, and 0.061, respectively. In addition, attempts to obtain a biradical TS using the UB3LYP method converged to the closed-shell RB3LYP solution. Therefore, we concluded that [8 + 2] saddle point **TS1a** can be described accurately as a closed-shell stationary point with no significant biradical character. The [4 + 2] cycloaddition via **TS2a** was calculated to be also feasible with a synchronicity value of Sy = 0.88, but with an activation barrier ca. 6 kcal/mol higher than that computed for the [8 + 2] process (Figure 2).

We also located another transition structure **TS3a** (Figure 2, Scheme 2) that is associated with a [1,5]$_s$ sigmatopic shift and connects the [4 + 2] cycloaduct **5a** with **3a**. This saddle point corresponds to a high barrier and relatively asynchronous process (Sy = 0.69). From these data, we conclude that the [8 + 2] cycloaduct imidazo[5,1,2-*cd*]indolizine **3a** will be the sole intermediate compound to be obtained under kinetic control.

A similar analysis was performed for the reaction between imidazo[1,2-*a*]pyrimidines **1b** and **2** (Figure 3). These reactants show two-electron pathways analogous to those found for the **1a** + **2** interaction. However, in this latter case, the energy gaps between the HOMO (**1b**)−LUMO (**2**) and LUMO (**1b**)−HOMO-1 (**2**) pairs are closer to each other, the former two-electron interaction being still the most important one. It is also interesting to note that the HOMO coefficient of C8 is quite low. Actually, all our attempts to locate **TS2b** corresponding to the [4 + 2] cycloaddition between **1b** and **2** met with no success, since all the starting geometries converged to **TS1b** upon optimization at the B3LYP/6-31G* level.

The main features of **TS1b** are shown in Figure 4 and are similar to those computed for **TS1a**. The synchronicity of the **1b** + **2** → **3b** is calculated to be Sy = 0.72, a value slightly higher than that found for the [8 + 2] cycloaddition starting from **1a**. As in the previous reaction, this process is calculated to be essentially barrierless at both the B3LYP and MO6-2X

(29) (a) Stowasser, R.; Hoffmann, R. *J. Am. Chem. Soc.* **1999**, *121*, 3414–3420. (b) Baeredens, E. J.; Gritsenko, O. V. *J. Phys. Chem. A* **1997**, *101*, 3583–5403. (c) Bickelhaupt, F. M.; Baerends, E. J. In: *Reviews in Computational Chemistry*; Lipkowitz, K. B., Boyd, D. B., Eds.; Wiley-VCH: New York, 2000; Vol. 15, pp 1−86.

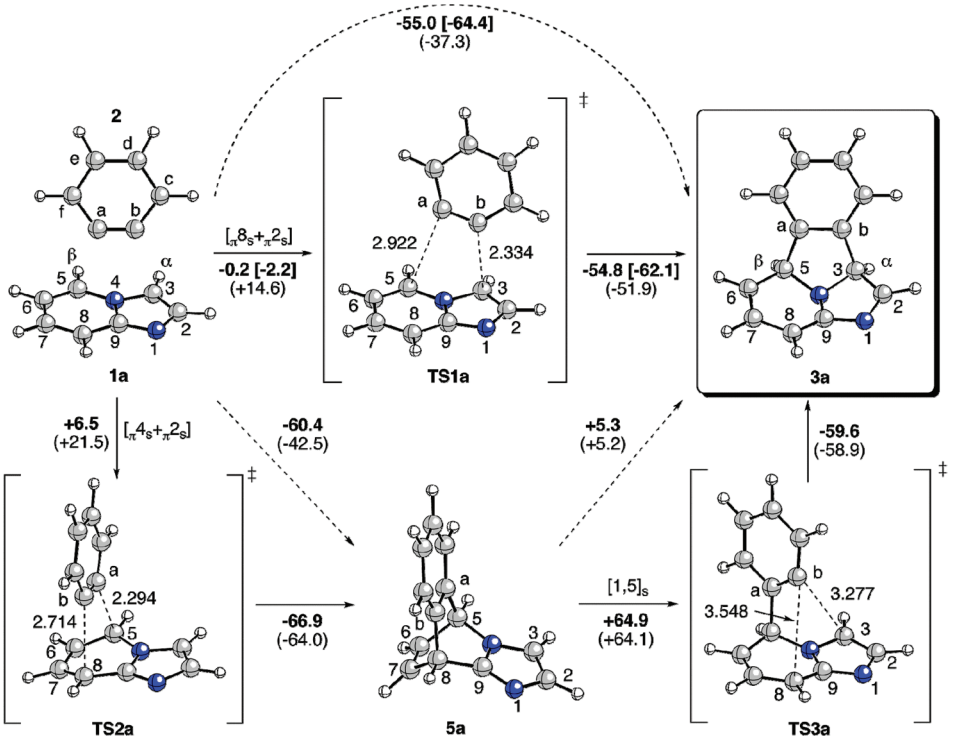

FIGURE 2. Stationary points (B3LYP/6-31G* level) found in the reaction between **1a** and **2**. Bond distances and energies are given in Å and in kcal/mol, respectively. Bold numbers over the arrows correspond to relative energies in kcal/mol calculated at the B3LYP/6-31G*+ΔZPVE level. Numbers in square brackets correspond to total energies calculated at the M06-2X/6-31G*//B3LYP/6-31G*+ΔZPVE level. Numbers in parentheses correspond to Gibbs energies at 80 °C (378.15 K) calculated at the B3LYP/6-31G*+ΔZPVE level.

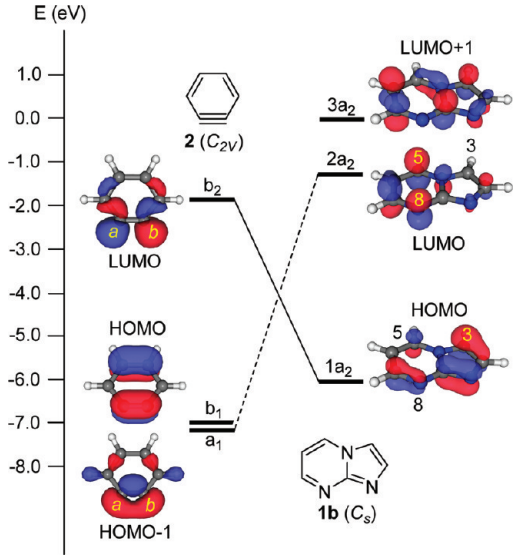

FIGURE 3. Kohn−Sham molecular orbitals of **1b** and **2**, calculated at the B3LYP/6-31G* level.

levels of theory. It is also interesting to note that [4 + 2] cycloaduct **5b** is calculated to be less stable than **3b**. Therefore, the high barrier associated with the $[1,5]_s$ sigmatropic shift connecting **3b** and **5b** via **TS3b**, as well as the endothermicity of the process indicate that, in this case, [8 + 2] cycloadduct *cis*-5a,9b-dihydro-2,3,9c-triazocyclopenta[*j*,*k*]-fluorene **3b** will be the only intermediate under both kinetic and thermodynamic control.

We next studied the aromatization reaction of [8 + 2] cycloaducts **3a**,**b** to yield compounds **4a**,**b** after loss of hydrogen (Scheme 2). The main features of saddle points **TS4a**,**b** associated with $[_{\sigma}2_s + _{\pi}6_s + _{\sigma}2_s]$ process, are gathered in Figure 5.

Our results indicate that this latter reaction has a significant energy barrier of ca. 46 kcal/mol for the **3a** → **4a** transformation. The analogue activation barrier for the **3b** → **4b** is even higher. These computed activation energies are consistent with those calculated for related systems in which the hydrogen departure takes place from methine groups connecting two cycles, i.e., [2,2]-type dehydrogenations, according to Radom's notation.[7] Houk et al.[7a] have shown that most of this activation barrier is related to the large distortion energy on going from the reactant to the transition structure. Both reactions are exothermic, the aromatization of the imidazole and pyridine (pyrimidine) rings of **3a**,**b** being the main driving force (vide infra). We have analyzed the evolution of the aromaticity of the different rings along the reaction coordinate. Since the NICS values computed ca. 0.75 Å above the molecular plane are a convenient magnetic criterion for aromaticity,[30] we computed the NICS for the four rings of the structures **3a**,**b**, **TS4a**,**b**, and **4a**,**b** at the different ring points of electron density as defined by Bader[31] and 0.75 Å above or below these ring points.[32] In order to

(30) Chen, Z.; Wannere, C. S.; Corminboeuf, C.; Puchta, R.; Schleyer, P. v. R. *Chem. Rev.* **2005**, *105*, 3842–3888.

(31) Bader, R. F. W. *Atoms in Molecules- A Quantum Theory*; Clarendon Press: Oxford, 1990; pp 12−52.

(32) (a) Morao, I.; Lecea, B.; Cossío, F. P. *J. Org. Chem.* **1997**, *62*, 7033–7036. (b) Morao, I.; Cossío, F. P. *J. Org. Chem.* **1999**, *64*, 1868–1874. (c) Cossío, F. P.; Morao, I.; Jiao, H.; Schleyer, P. v. R. *J. Am. Chem. Soc.* **1999**, *121*, 6737–6746.

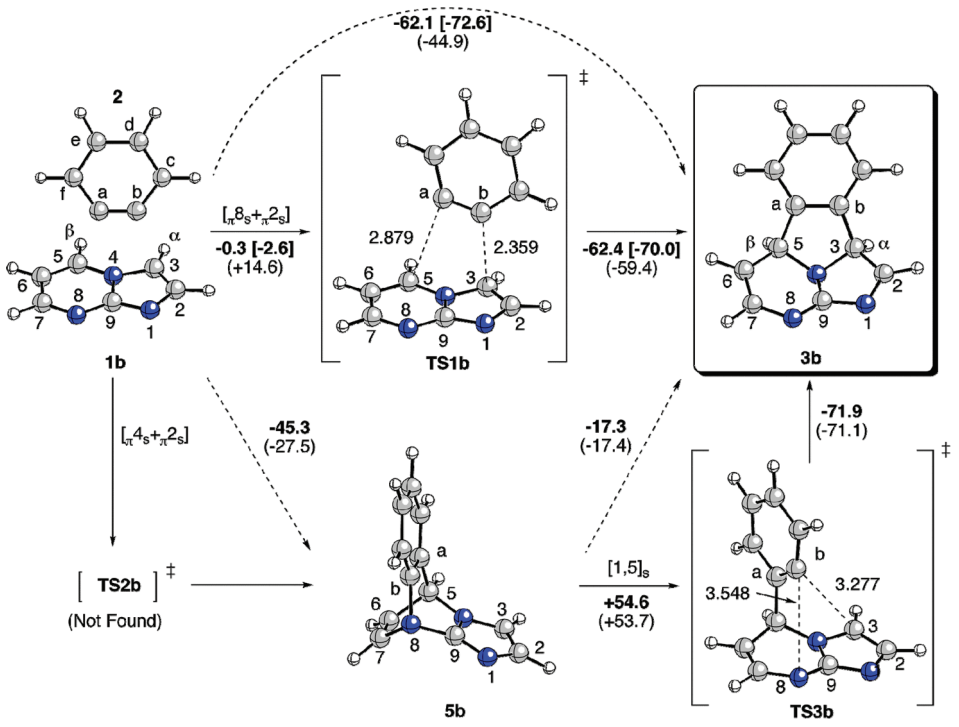

FIGURE 4. Stationary points (B3LYP/6-31G* level) found in the reaction between **1b** and **2**. Bond distances and energies are given in Å and in kcal/mol, respectively. Bold numbers over the arrows correspond to relative energies in kcal/mol calculated at the B3LYP/6-31G*+ΔZPVE level. Numbers in square brackets correspond to total energies calculated at the M06-2X/6-31G*//B3LYP/6-31G*+ΔZPVE level. Numbers in parentheses correspond to Gibbs energies at 80 °C (378.15 K) calculated at the B3LYP/6-31G*+ΔZPVE level.

avoid local diamagnetic shielding effects induced by the C−H bonds being cleaved, these points were computed on the opposite side of these bonds (see Figure 5).

For compounds **3a**,**b** the only π-aromatic ring that exhibits large negative NICS values is the phenyl moiety incorporated during the [8 + 2] cycloaddition. The remaining rings are nonaromatic according to the low NICS (0.75) values. In contrast, both **TS4a** and **TS4b** saddle points exhibit large negative values for the central five-membered ring, namely the cyclic structure that is being transformed in the $[_o2_s + _\pi6_s + _o2_s]$ process. The computed NICS (0) and NICS (0.75) values are comparable with those found for the phenyl ring and larger in absolute value than those calculated for the remaining rings. These results indicate that the concerted cleavage of the C3−Hα and C5−Hβ bonds generates a strong diamagnetic ring current along the central and imidazo[1,2-*a*]pyridine(pyrimidine) rings, a process associated with thermally allowed pericyclic reactions.[32] The calculated synchronicities for both **3a** → **4a** and **3b** → **4b** transformations, Sy = 0.88 and 0.87, respectively, also agree with highly synchronous concerted mechanisms associated with aromatic transition structures **TS4a**,**b**.

The electron count in the assessment of the aromatic character of compounds **4a**,**b** is ambiguous. If the inner nitrogen atom does not participate in the electronic circulation, there would be a polyunsaturated 14 π-electron aromatic array. (Figure 6, resonance forms I and II). In this circulation along the periphery of **4a**,**b** (Figure 6, state A) strong delocalization across the Ca−C5 and Cb−C3 bonds is required, as indicated in resonance form II of Figure 6. This delocalization is not observed in the B3LYP wave functions of **4a**,**b**, since the respective bond orders are ca. 1.1 for these bonds. Instead, the NBO analysis indicates a π-bond between N4 and C9, with an occupation of 1.75e. This results in a NBO charge of −0.34 for N4, whereas that of N1 is −0.49. This difference in the electrostatic charge is readily appreciated in the electrostatic potential of **4a** projected onto the electric density, as represented in Figure 6. The π(N4═C9) localized bond interacts strongly with other π systems of rings. Therefore, instead of a sole 14π-electron aromatic system, compounds **4a**,**b** are better described as molecules possessing two independent aromatic moieties: one 6π-electron system associated with the phenyl group and another 10π-electron bicyclic moiety associated with the imidazo[1,5-*a*]-pyridine (pyrimidine) rings. These two separated π-systems can also be observed in Figure 6C and can be associated with resonance forms indicated in Figure 6B. The NICS values also agree with this two-ring current model (see Figure 5). Wudl et al. reported similar observations on the electronic distribution in indolizino[3,4,5-*ab*]isoindole.[6b]

We have also studied the above-mentioned reactions experimentally. In a first series of experiments, the reaction between **1a** and the benzene precursor 2-(trimethylsilyl)phenyl trifluoromethanesulfonate **6a**[33] was carried out (Scheme 3). Microwave-promoted ortho-elimination of **6a** in the presence of CsF and subsequent in situ $[_\pi8_s + _\pi2_s]$ cycloaddition of the intermediate *o*-benzyne **2** with **1a** followed by $[_o2_s + _\pi6_s + _o2_s]$ reaction yields compound **4a** in 39% isolated overall yield (Scheme 3). When the reaction was carried out by classical

(33) (a) Himeshima, Y.; Sonoda, T.; Kobayashi, H. *Chem. Lett.* **1983**, 1211–1214. (b) Shi, F.; Waldo, J. P.; Chen, Y.; Larock, R. C. *Org. Lett.* **2008**, *10*, 2409–2412. (c) Akai, S.; Ikawa, T.; Takayanagi, S.; Morikawa, Y.; Mori, S.; Tsubakiyama, M.; Egi, M.; Wada, Y.; Kita, Y. *Angew. Chem., Int. Ed.* **2008**, *47*, 7673–7676.

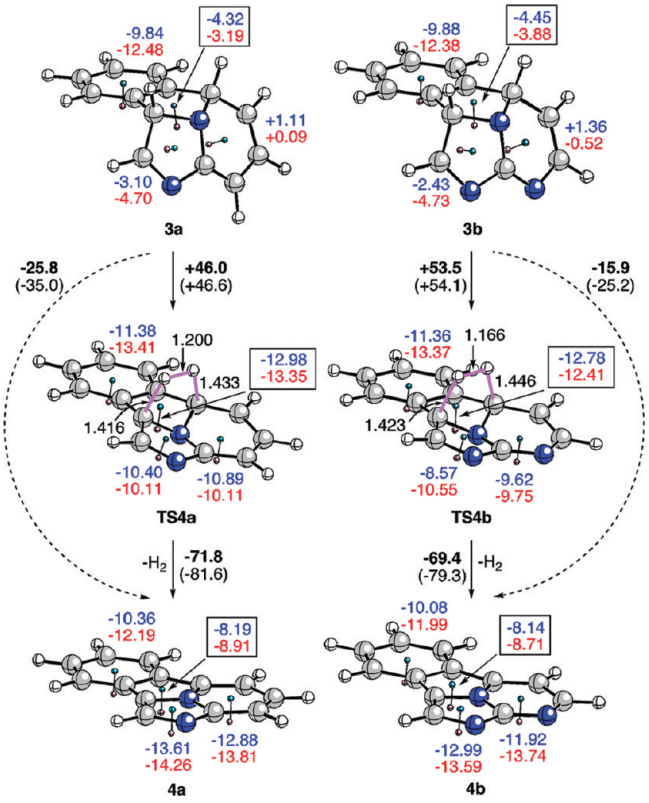

FIGURE 5. Stationary points (B3LYP/6-31G* level) found in the aromatization reactions of **3a**,**b** to yield **4a**,**b**. Bond distances and energies are given in Å and in kcal/mol, respectively. Bold numbers over the arrows correspond to relative energies in kcal/mol calculated at the B3LYP/6-31G*+ΔZPVE level. Numbers in parentheses correspond to Gibbs energies at 80 °C (378.15 K) calculated at the B3LYP/6-31G*+ΔZPVE level. Numbers on the rings correspond to the NICS (in ppm, GIAO/6-31G*//B3LYP/6-31G* level) computed at the ring points of electron density and 0.75 Å below these points, respectively. These points are represented as small blue and pink spheres, respectively.

heating, only traces of **4a** could be observed by NMR in the crude reaction mixture. Under microwave irradiation, we were unable to detect intermediate **3a**. In order to assess the kinetic stability of this intermediate, we carried out CP-MD simulations (vide supra). As can be appreciated in Figure 7, no C5−Hα or Ca−C5 bond cleavage was observed after 75 ps of simulation. Therefore, we conclude that cycloadducts **3** should be persistent, isolable intermediates. However, the characterization of these intermediates under the actual reaction conditions is very difficult to achieve.

In a second series of experiments, we prepared compounds **9a**−**i** by direct reaction between 2-aminopyridine **7a** or 2-aminopyrimidine **7b** and α-bromoacetophenones **8b**−**i** or ethyl bromopyruvate **8a** (Scheme 4).[8,34] In order to extend the previous computational work to 2-substituted compounds **9**, we investigated the [8 + 2] reaction between 2-phenylimidazo[1,2-*a*]pyridine **9b** and benzyne **2**. The results are gathered in Figure 8. As can be appreciated

(34) (a) Yadav, J. S.; Reddy, B. V. S.; Rao, Y. G.; Srinivas, M.; Narsaiah, A. V. *Tetrahedron Lett.* **2007**, *48*, 7717–7720. (b) Ueno, M.; Togo, H. *Synthesis* **2004**, *16*, 2673–2677. (c) Katritzky, A. R.; Qiu, G.; Cong, Q.-H.; He, H.-Y.; Steel, M. J. *J. Org. Chem.* **2000**, *65*, 9201–9205. (d) Xie, Y.-Y. *Synth. Commun.* **2005**, *35*, 1741–1746.

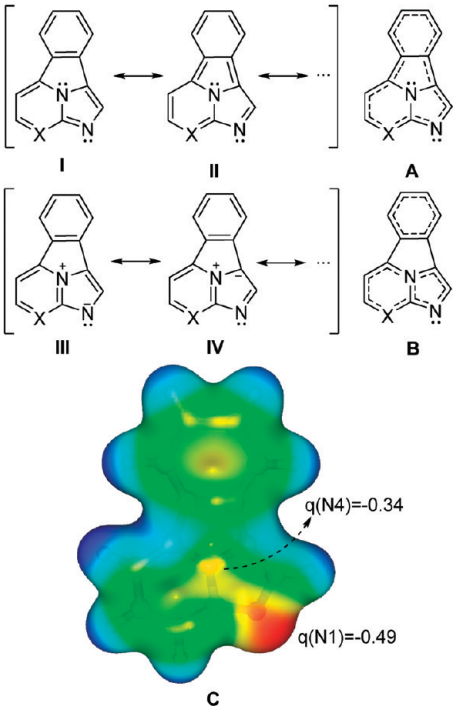

FIGURE 6. (A and B) Alternative resonance forms associated with delocalized representations corresponding to **4a** (X = CH) and **4b** (X = N). (C) Electrostatic potential of **4a** projected onto electron density (isosurface value: 0.01 au). Colors range from +0.059 kcal/mol (blue) to −0.106 kcal/mol (red). Notice the two green regions associated with the electronic delocalization represented in B (see text).

SCHEME 3. Microwave-Assisted Reaction between Imidazo-[1,2-*a*]pyridine 1a and Benzene Precursor 6a[a]

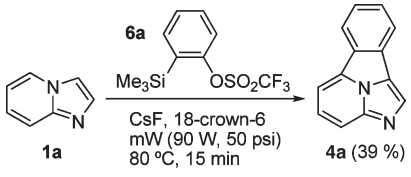

[a]Numbers in parentheses corresponds to the yield of isolated pure compound **4a**.

from the 3D-projected potential energy hypersurface, the [8 + 2] reaction involving benzyne and the 2-substituted reactant is essentially barrierless in terms of total energy, with an asynchronous TS whose features are similar to those found for **TS1a**. Similarly, the elimination of hydrogen occurs via a synchronous transition structure very similar to **TS4a**.

We observed that the reaction between compounds **9a**−**g** and the benzyne precursor **6a** takes place with moderate overall yields under microwave irradiation. When classical heating was used, no appreciable formation of products **10** was observed. In addition, only the aromatized products were obtained. As in the previous case, we were unable to isolate and fully characterize the intermediate [8 + 2] cycloadducts. The structures of compounds **4a** and **10a**−**i** were determined by their spectroscopic and analytical properties. In the case of compounds **10c**, the corresponding structure

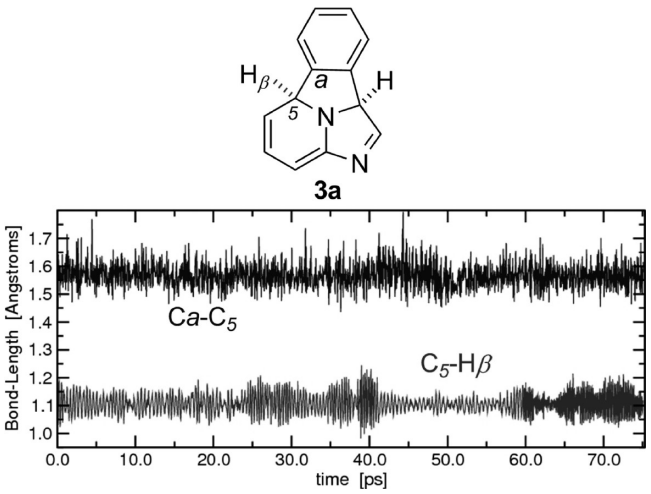

FIGURE 7. CP-MD simulation of intermediate **3a**. Upper and lower lines correspond to the evolution of Ca−C5 and C5−H_β bonds, respectively.

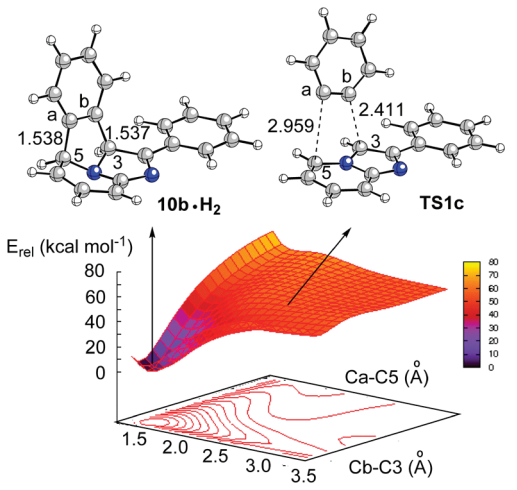

FIGURE 8. B3LYP/6-31G* relaxed scan corresponding to the interaction between benzyne **2** and compound **9b** (Scheme 4). Bond distances are given in Å.

SCHEME 4. Formation of Tetracyclic Compounds 10a−i from 9a−i and Benzyne Precursor 6a under Microwave Irradiation[a]

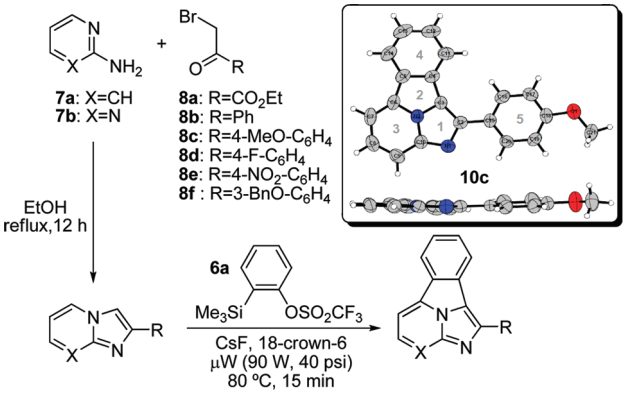

9a: X=CH; R=CO_2Et (58 %)
9b: X=CH; R=Ph (78 %)
9c: X=CH; R=4-MeO-C_6H_4 (84 %)
9d: X=CH; R=4-F-C_6H_4 (72 %)
9e: X=CH; R=4-NO_2-C_6H_4 (75 %)
9f : X=CH; R=3,5-$(BnO)_2$-C_6H_4 (46 %)
9g: X=N; R=Ph (52 %)
9h: X=N; R=4-MeO-C_6H_4 (86 %)
9i : X=N; R=4-F-C_6H_4 (71 %)

10a: X=CH; R=CO_2Et (51 %)
10b: X=CH; R=Ph (74 %)
10c: X=CH; R=4-MeO-C_6H_4 (39 %)
10d: X=CH; R=4-F-C_6H_4 (49 %)
10e: X=CH; R=4-NO_2-C_6H_4 (51 %)
10f : X=CH; R=3,5-$(BnO)_2$-C_6H_4 (49 %)
10g: X=N; R=Ph (58 %)
10h: X=N; R=4-MeO-C_6H_4 (54 %)
10i : X=N; R=4-F-C_6H_4 (38 %)

[a]The diagram corresponding to the X-ray diffraction analysis structure of **10c** is also included. Numbers in parentheses correspond to yields of isolated pure compounds.

was confirmed by X-ray diffraction analysis.[35] It is noteworthy that the experimental structure of **10c** shows a planar molecule whose geometric parameters are consistent with the computed ones.

We next investigated the regiochemistry of the reaction. Reaction of either **9c** or **9h** with benzyne precursor 3-methoxy-2-(trimethylsilyl)phenyl triflate **6b** resulted in the exclusive formation of cycloadducts **10j**,**k**, in which the methoxy group stemming from **9b** occupies the 6-position of both bicyclic systems (Scheme 5). In contrast, when benzyne

(35) CCDC 741416 contains the supplementary crystallographic data for compound **10c**. These data can be obtained free of charge via www.ccdc.cam.ac.uk/data_request/cif, by emailing data_request@ccdc.cam.ac.uk, or by contacting The Cambridge Crystallographic Data Centre, 12 Union Rd, Cambridge CB2 1EZ, UK; fax: +44 1223 336033.

SCHEME 5. Regiochemistry of the Reaction between Compounds 9c,h and Benzyne Precursors 6b,c[a]

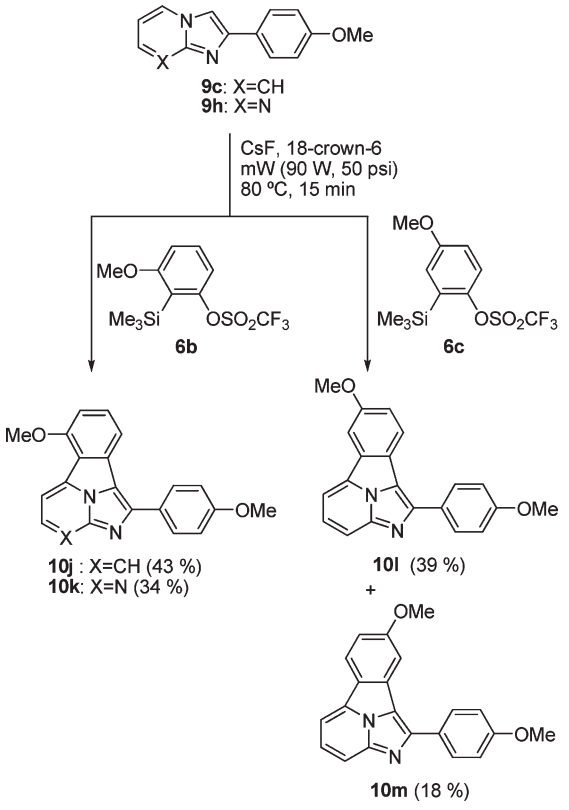

[a]Numbers in parentheses correspond to yields of isolated pure compounds.

precursor **6c** reacted with **8c**, a ca. 2:1 mixture of 7- and 8- substituted regioisomers **10l** and **10m** was obtained. This lack of selectivity is consistent with the reaction profile calculated for the [8 + 2] cycloaddition step, which determines the regiochemistry of the reaction. The high regioselectivity observed for the reaction with triflate **6b** is also in agreement with the high asynchronicity computed for the

TABLE 1. Selected Photophysical Parameters of Compounds 9 and 10

compd	λ_{exc}[a] (nm)	λ_{em}[b] (nm)	$\Delta\lambda$[c] (nm)	Φ_f[d]	τ[e] (ns)
9a	316	357	41	0.27	3.42
10a	408	419	11	0.09	n.m.
9c	331	379	48	0.51	3.66
10c	419	428	9	0.37	5.16
9d	326	372	46	0.46	3.90
10d	418	425	7	0.38	5.68
9e	409	570	161	0.03	1.26
10e	419	589	170	0.10	1.66
9i	349	410	61	0.47	4.95
10i	419	481	62	0.59	9.56

[a]Excitation wavelength. [b]Emission wavelength. [c]Stokes shift, computed as $\Delta\lambda = \lambda_{exc} - \lambda_{em}$. [d]Fluorescence quantum yield, computed in CH_2Cl_2 at 25 °C (see the Supporting Information). [e]Time-domain excited-state lifetime, measured by time correlated simple photon counting (see the Supporting Information).

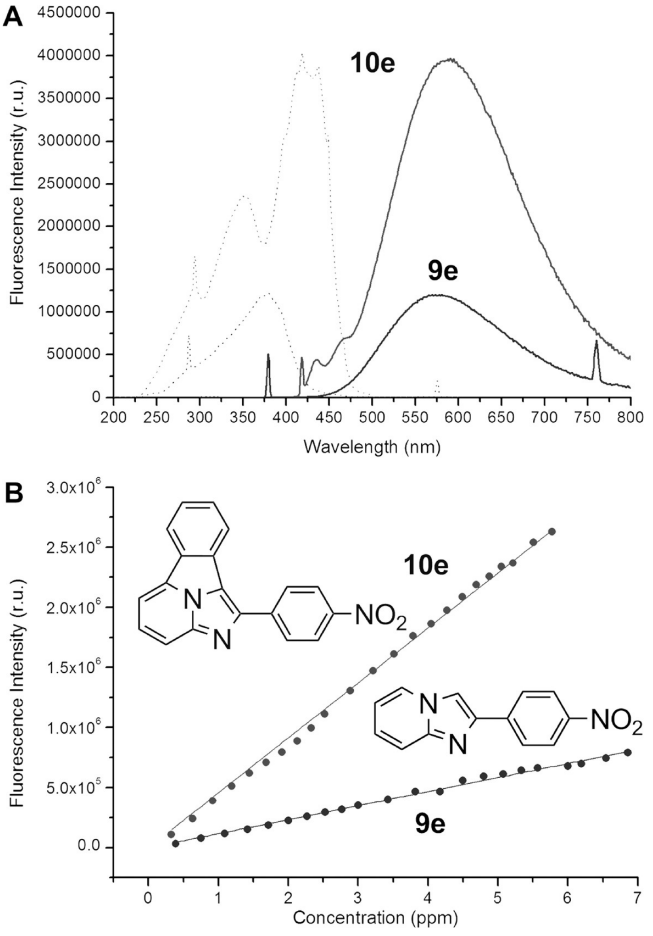

FIGURE 9. (A) Excitation (dotted lines) and emission (solid lines) spectra of compounds **10e** and **9e**. Both sets of spectra were recorded at a concentration of 10.2 ppm. (B) Plots of fluorescence intensity vs concentration for **10e** and **9e**.

[8 + 2] cycloaddition step (see Figures 2 and 4). Actually, all our attempts to calculate the transition structure leading to the nonobserved regiosomer of **10j** were unfruitful. The structures of compounds **10j**,**k** and **10l**,**m** were elucidated on the basis of their spectroscopic and analytical properties and by selective nuclear Overhauser experiments on the ^{1}H NMR spectra, with a mixing time of 300 ms (see the Supporting Information).

Finally, we studied the photophysical properties of compounds **10** and their differences with respect to bicyclic compounds **9**. The results are gathered in Table 1. It is observed that the electron-withdrawing ethoxycarbonyl group in **10a** quenches the fluorescence, whereas in the remaining cases, which include 1-aryl groups, an enhancement of fluorescence intensity is observed. In Figure 9, the plots of fluorescence intensity vs concentration are reported for compounds **9e** and **10e**. As can be seen, within the concentration range of 1−7 ppm the Beer−Lambert law is followed. The emission wavelengths of compounds **10** lie in the range ca. 420−560 nm, whereas those of compounds **9** are somewhat lower. Compound **10e** exhibits a considerable Stokes shift (Table 1, Figure 10). This compound is interesting since it emits at 589 nm, the highest value among the compounds studied. It is noteworthy that the 2,3,9c-triazocyclopenta[*j*,*k*]fluorene scaffold present in **10i** induces the highest quantum yield (Φ_f) among the compounds studied. This quantum yield of **10i** is comparable to that of quinine sulfate. Its precursor **9i** also exhibits relatively high values of Φ_f and τ (Table 1). The same trend is observed in compound **10d**, in which the 1-(4-fluorophenyl) group is attached to a benzo[*a*]imidazo[5,1,2-*cd*]indolizine tetracyclic system.

Conclusions

From the computational and experimental study reported in this work the following conclusions can be drawn: (i) The reaction between benzyne and imidazo[1,2-*a*]pyridine (pyrimidine) **1a**,**b** to form 5a,9b-dihydrobenzo[*a*]imidazo-[5,1,2-*cd*]indolizine **3a** and 5a,9b-dihydro-2,3,9c-triazocyclopenta[*j*,*k*]fluorene **3b** takes place via a highly asynchronous concerted [$_\pi 8_s + _\pi 2_s$] mechanism. This process is barrierless in terms of total energy. (ii) The aromatization reaction of compounds **3a**,**b** to yield benzo[*a*]imidazo[5,1,2-*cd*]indolizine **4a** and 2,3,9c-triazocyclopenta[*j*,*k*]fluorene **4b** is concerted and highly synchronous. (iii) The reaction can be carried out experimentally under microwave irradiation and using 2-(trimethylsilyl) phenyl triflates as benzyne precursors. (iv) Under certain conditions, the reaction can be completely regioselective. (v) The final products are aromatic, blue light emitting fluorescent molecules whose fluorescence intensity, quantum yields, and excited-state lifetimes are enhanced with respect to the starting bicyclic molecules.

Experimental Section

General Methods. Microwave irradiations were conducted in a focused microwave reactor CEM Discover at the power and for the time indicated. NMR data were obtained using TMS as an internal standard. Column chromatography was carried out with 230−400 mesh silica gel. Reagents were purchased from commercial suppliers or prepared according to literature procedures.

Experimental Procedure for the Synthesis of Compounds 4a and 10a−g. Benzyne precursor **6** (0.2 mmol) was added to a mixture of **1a** or **9** (0.6 mmol), 18-crown-6 (0.11 g, 0.4 mmol), and CsF (0.4 mmol). The resulting mixture was irradiated in a monomode microwave reactor at 80 °C, 90 W, and 40 psi for 15 min. The resulting mixture was dissolved in ethyl acetate and evaporated. The residue was purified by flash chromatography (ethyl acetate/hexanes 1:2) to yield the corresponding pure product **4a** or **10**.

Benzo[*a*]imidazo[5,1,2-*cd*]indolizine (4a). This compound was prepared from **1a** and **6a**: yield 39%; mp 173−175 °C; IR (KBr) ν_{max} cm^{-1} = 3054, 2926; ^{1}H NMR (500 MHz, $CDCl_3$) δ = 8.51 (s, 1H), 8.37 (d, J = 8.0, 1H), 8.22 (d, J = 8.0, 1H), 8.12 (d, J = 8.4, 1H), 8.07 (d, J = 7.2, 1H), 8.01−7.92 (m, 1H), 7.76 (t, J = 7.5, 1H), 7.61 (t, J = 7.6, 1H); ^{13}C NMR (500 MHz, $CDCl_3$) δ = 139.6, 132.2, 131.4, 130.8, 129.2, 128.6, 126.30, 124.0, 124.3, 123.0, 121.0, 114.0, 109.1. Anal. Calcd for $C_{13}H_8N_2$: C, 81.2; H, 4.2; N, 14.6. Found: C, 81.4; H, 4.1; N, 14.6.

Ethyl Benzo[*a*]imidazo[5,1,2-*cd*]indolizine-1-carboxylate (10a). This compound was prepared from **9a** and **6a**: yield 51%; mp 78−79 °C; IR (KBr) ν_{max} cm^{-1} = 3059, 2924, 1727, 1309, 1082; ^{1}H NMR (500 MHz, MeOD) δ = 8.56 (d, J = 8.0, 1H), 8.50 (d, J = 8.0, 1H), 8.30 (d, J = 6.8, 1H), 8.19−8.09 (m, 2H), 7.85 (t, J = 7.6, 1H), 7.74 (t, J = 7.7, 1H), 4.64 (q, J = 7.1, 2H), 1.59 (t, J = 7.1, 3H); ^{13}C NMR (500 MHz, $CDCl_3$) δ = 164.0, 139.1, 134.39, 132.7, 132.3, 130.3, 129.4, 128.6, 127.0, 123.9, 123.4, 116.6, 110.8, 61.6, 14.4. Anal. Calcd for $C_{16}H_{12}N_2O_2$: C, 72.7; H, 4.6; N, 10.6. Found: C, 72.8; H, 4.5; N, 10.8.

1-Phenyl-2,3,9c-triazacyclopenta[*jk*]fluorene (10g). This compound was prepared from **9g** and **6a**: yield 58%; mp 177−178 °C; IR (KBr) ν_{max} cm^{-1} = 3046, 2923, 2849; ^{1}H NMR (500 MHz, $CDCl_3$) δ = 9.08 (d, J = 4.8, 1H), 8.37 (d, J = 7.5, 2H), 8.28 (d, J = 8.2, 2H), 7.84 (d, J = 4.8, 1H), 7.78 (t, J = 7.6, 1H), 7.60 (t, J = 7.5, 2H), 7.56−7.47 (m, 2H); ^{13}C NMR (500 MHz, $CDCl_3$) δ = 150.5, 148.9, 146.2, 135.1, 134.0, 131.7, 130.7, 130.6, 130.1, 129.3, 128.8, 125.5, 124.9, 121.3, 119.0, 104.6. Anal. Calcd for $C_{18}H_{11}N_3$: C, 80.3; H, 4.1; N, 15.6. Found: C, 80.2; H, 4.0; N, 15.5.

7- and 8-Methoxy-1-(4-methoxyphenyl)benzo[*a*]imidazo[5,1,2-*cd*]indolizine (10l and 10m). These compounds were prepared as a mixture of diastereomers from **9c** and **6c** and purified by column chromatography. **10l**: yield 39%; mp 157−159 °C; IR (KBr) ν_{max} cm^{-1} = 3094, 2920, 2844, 1235, 1183, 1067, 1029; ^{1}H NMR (500 MHz, $CDCl_3$) δ = 8.69 (d, J = 7.7, 1H), 8.37−8.22 (m, 5H), 7.90 (s, 1H), 7.50 (dd, J = 8.7, 1.7, 1H), 7.25 (d, J = 8.6, 2H), 4.08 (s, 3H), 3.98 (s, 3H); ^{13}C NMR (500 MHz, $CDCl_3$) δ = 166.9, 164.7, 139.1, 138.2, 138.1, 137.3, 136.8, 134.2, 127.1, 126.5, 124.6, 123.1, 120.0, 117.3, 114.0, 111.6, 60.3, 59.9. Anal. Calcd for $C_{21}H_{16}N_2O_2$: C, 76.8; H, 4.9; N, 8.5. Found: C, 77.0; H, 4.7; N, 8.5. **10m**: yield 18%; mp 161−162 °C; IR (KBr) ν_{max} cm^{-1} = 2914, 2856, 1256, 1230, 1171, 1032; ^{1}H NMR (500 MHz, $CDCl_3$) δ = 8.31 (d, J = 8.7, 2H), 8.28 (d, J = 8.7, 1H), 7.95 (dd, J = 6.0, 2.9, 1H), 7.92−7.87 (m, 2H), 7.85 (d, J = 2.1, 1H), 7.21 (dd, J = 8.8, 2.2, 1H), 7.16 (d, J = 8.7, 2H), 4.04 (s, 3H), 3.94 (s, 3H); ^{13}C NMR (500 MHz, CDCl3) δ = 161.6, 161.1, 147.3, 140.5, 131.3, 131.0, 130.3, 128.1, 127.1, 125.6, 124.8, 115.2, 113.7, 112.3, 107.9, 104.8, 56.4, 56.1. Anal. Calcd for $C_{21}H_{16}N_2O_2$: C, 76.8; H, 4.9; N, 8.5. Found: C, 76.7; H, 4.9; N, 8.4.

Acknowledgment. We thank the Spanish Ministerio de Ciencia e Innovación (MCINN, Grant Nos. CTQ 2007-67528 and CTQ2008-00959 and Ingenio-Consolider C5D2007-00006) and the UPV/EHU-GV/EJ (Grant No. IT-324-07) for financial support. We also thank SGIker technical support for computational resources, X-ray analysis, and NMR spectra (MCINN, GV/EJ, European Social Fund.). M.A. and A.D.-C. acknowledge their GV/EJ and MCINN fellowships, respectively.

Supporting Information Available: Complete experimental procedures for all remaining compounds, including ^{1}H NMR, COSY, and ^{13}C NMR spectra of all new compounds. NOE experiments for compounds **10j**−**m**. Thermal ellipsoid plot for the crystal structure of compound **10c**. Complete reference 9. Cartesian coordinates, harmonic analysis data, and energies for all the stationary points discussed in the text. This material is available free of charge via the Internet at http://pubs.acs.org.